

Spectral split in prompt supernova neutrino burst: Analytic three-flavor treatment

Basudeb Dasgupta,¹ Amol Dighe,¹ Alessandro Mirizzi,² and Georg G. Raffelt²

¹*Tata Institute of Fundamental Research, Homi Bhabha Road, Mumbai 400005, India*

²*Max-Planck-Institut für Physik (Werner-Heisenberg-Institut), Föhringer Ring 6, 80805 München, Germany*

(Dated: 10 January 2008, revised 28 April 2008)

The prompt ν_e burst from a core-collapse supernova (SN) is subject to both matter-induced flavor conversions and strong neutrino-neutrino refractive effects. For the lowest-mass progenitors, leading to O-Ne-Mg core SNe, the matter density profile can be so steep that the usual MSW matter effects occur within the dense-neutrino region close to the neutrino sphere. In this case a “split” occurs in the emerging spectrum, i.e., the ν_e flavor survival probability shows a step-like feature. We explain this feature analytically as a “MSW prepared spectral split.” In a three-flavor treatment, the step-like feature actually consists of two narrowly spaced splits. They are determined by two combinations of flavor-lepton numbers that are conserved under collective oscillations.

PACS numbers: 14.60.Pq, 97.60.Bw

I. INTRODUCTION

The neutrino flux streaming off a collapsed supernova (SN) core is an intriguing astrophysical case where flavor transformations depend sensitively on some of the unknown elements of the leptonic mixing matrix [1, 2]. Since the conversion probabilities depend also on the time-dependent matter profile, a high-statistics SN neutrino observation may also reveal, for example, signatures for shock-wave propagation [3, 4, 5, 6, 7, 8, 9]. While galactic SNe are rare, various ongoing and future experimental programmes depend on large detectors that, besides their main purpose, are also sensitive to SN neutrinos [10]. Therefore, understanding the flavor evolution of a SN neutrino signal remains of topical interest.

The flavor transformation probabilities not only depend on the matter background, but also on the neutrino fluxes themselves: neutrino-neutrino interactions provide a nonlinear term in the equations of motion [11, 12] that causes collective flavor transformations [13, 14, 15, 16, 17, 18, 19, 20, 21, 22]. Only recently has it been fully appreciated that in the SN context these collective effects give rise to qualitatively new phenomena [23, 24, 25, 26, 27, 28, 29, 30, 31, 32, 33, 34, 35, 36].

One peculiar aspect of the expected SN neutrino fluxes is the hierarchy $F_{\nu_e} > F_{\bar{\nu}_e} > F_{\nu_\mu} = F_{\bar{\nu}_\mu} = F_{\nu_\tau} = F_{\bar{\nu}_\tau}$ so that there is an excess flux of $\nu_e\bar{\nu}_e$ pairs over those of the other flavors. The nonlinear terms cause a collective transformation $\nu_e\bar{\nu}_e \rightarrow \nu_x\bar{\nu}_x$, where ν_x is a specific linear combination of ν_μ and ν_τ . The detailed dynamics of this transition is complicated and several important aspects are only numerically observed, not analytically understood. Still, the most crucial point is that the pair transformation $\nu_e\bar{\nu}_e \rightarrow \nu_x\bar{\nu}_x$ proceeds collectively much faster than ordinary pair annihilation, so we have to contend with a “speed-up phenomenon” [21, 22]. The pair process does not violate flavor-lepton number. Being an instability in flavor space, it proceeds efficiently even for a very small mixing angle.

A very different situation prevails in the interior of a SN core where the ν_e distribution is determined by a large

chemical potential that enhances the ν_e density and suppresses the $\bar{\nu}_e$ density relative to that of ν_x and $\bar{\nu}_x$ so that collective pair conversions are not possible. Neutrino-neutrino interactions are strong, but their only impact is to synchronize the flavor oscillations (“self-maintained coherence”). Significant flavor transformation here requires a violation of flavor-lepton number. However, the high density of ordinary matter suppresses the effective mixing angles between ν_e and the other flavors. Therefore, in the interior of a SN core the individual flavor-lepton numbers are almost perfectly conserved [37].

Immediately after collapse, the SN emits a prompt ν_e burst that arises from the de-leptonization (neutronization) of the outer layers of the collapsed core. Once more we have a strongly enhanced ν_e and a suppressed $\bar{\nu}_e$ flux relative to the other flavors [38]. Once more, collective pair transformations are not possible: efficient flavor conversion requires a large violation of flavor-lepton number and is not possible if the ordinary matter density is large. At some distance from the neutrino sphere, the ν_e flux encounters the usual MSW level crossings driven by the atmospheric neutrino mass difference Δm_{atm}^2 (H cross-

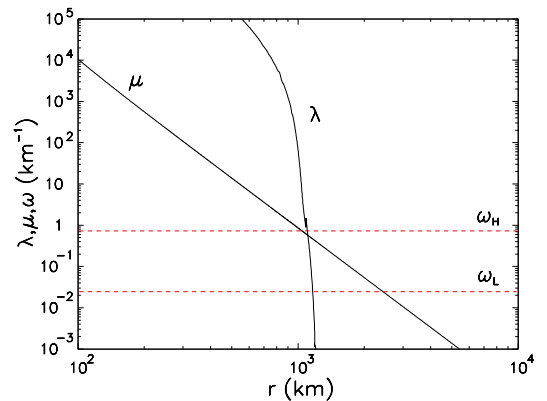


FIG. 1: Profile of the matter potential λ and the effective neutrino-neutrino interaction potential μ for an O-Ne-Mg core collapse SN [39, 40, 41, 42].

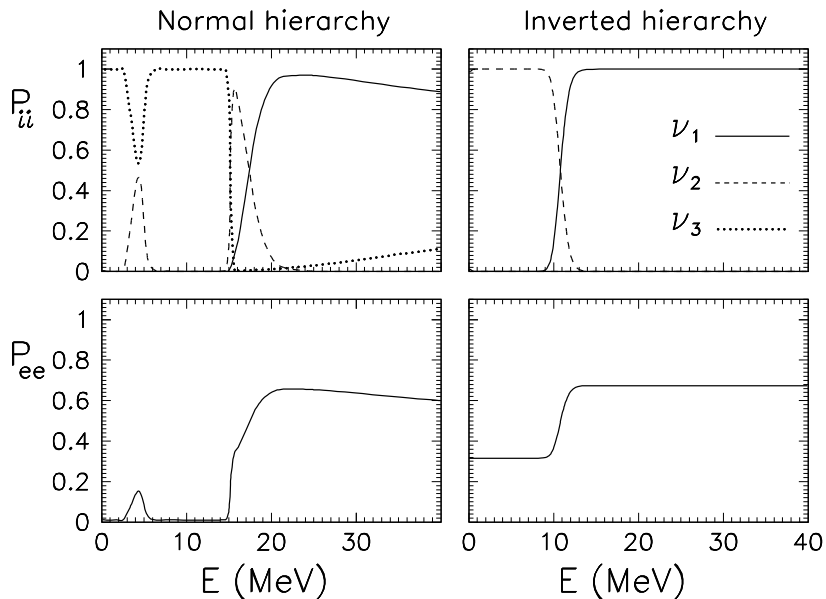


FIG. 2: Mass eigenstate fractions P_{ii} as well as the ν_e survival probabilities far away from the star, numerically computed using the SN model of Fig. 1 and an initial flux of pure ν_e .

ing) and by the solar mass difference Δm_{\odot}^2 (L crossing), leading to the usual resonant transformations [1, 38].

An interesting new case is motivated by the insight that SNe with the lowest progenitor masses of 8–10 M_{\odot} , encompassing perhaps 30% of all cases, collapse before forming an iron core, the class of O-Ne-Mg core collapse SNe [39, 40, 41, 42]. In state-of-the-art numerical simulations these SNe explode even in a spherically symmetric treatment (convection plays no role), largely because their envelope mass is very small. By the same token, the matter density profile above the core is very steep even at the time of core bounce. In this case the H and L level crossings occur very close to the neutrino sphere and may well lie deeply within the collective neutrino region. This is illustrated in Fig. 1 where we show $\lambda(r) = \sqrt{2}G_{\text{F}}n_e(r)$ of an O-Ne-Mg core progenitor star [39, 40, 41]. We also show $\omega_{\text{H}} = \langle \Delta m_{\text{atm}}^2 / 2E \rangle$ and $\omega_{\text{L}} = \langle \Delta m_{\odot}^2 / 2E \rangle$ as horizontal lines, where the average is over the Fermi-Dirac spectrum of neutrino energies described below. The intersection of $\lambda(r)$ with these lines indicates the locations of the H and L level crossings.

In Fig. 1 we also show the effective neutrino-neutrino interaction potential $\mu = \sqrt{2}G_{\text{F}}F_{\nu_e} \langle 1 - \cos \theta \rangle_{\text{eff}}$, where θ is the angle between different neutrino trajectories and $\langle \dots \rangle_{\text{eff}}$ stands for a suitable average. At large distances, μ scales approximately as r^{-4} . Collective neutrino effects driven by Δm_{atm}^2 are important for $\mu(r) \gtrsim \omega_{\text{H}}$ and driven by Δm_{\odot}^2 for $\mu(r) \gtrsim \omega_{\text{L}}$.

Duan et al. [34] have recently shown that in this case the interplay of ordinary MSW conversions with collective oscillations leads to interesting effects. We start with a pure ν_e flux with a Fermi-Dirac spectrum ($\langle E_{\nu_e} \rangle = 11$ MeV, degeneracy parameter $\eta = 3$), and numerically calculate the mass eigenstate fractions P_{ii} and

the ν_e survival probabilities P_{ee} far away from the star, as shown in Fig. 2. These plots are in qualitative agreement with the corresponding curves in Fig. 2 of Ref. [34]. However, our P_{ee} is constructed as an incoherent sum of the mass fractions, thus representing the physical situation far away from the star, where the oscillatory features seen in Duan et al.’s P_{ee} have disappeared.

In inverted hierarchy, one observes that the neutrinos emerging from the star are in the ν_2 state at low energies and in the ν_1 state at high energies, with the transition taking place around $E \approx 12$ MeV. This results in a step function in energy for P_{ee} .

In the normal hierarchy, the neutrinos emerging from the star are in ν_1 state for $E \gtrsim 17$ MeV, in ν_2 state for $15 \text{ MeV} \lesssim E \lesssim 17$ MeV, and in the ν_3 state for $E \lesssim 15$ MeV. The bump seen around 5 MeV is due to an abrupt change in the matter density profile used for the computation (see [34] for details), and we do not address it here. The transition at $E \approx 15$ MeV is rather sharp, however the one at $E \approx 17$ MeV is not as abrupt. This results in a two-step function for P_{ee} , with the step at $E \approx 17$ MeV somewhat smoothed out.

Broadly, this is an example of a “MSW prepared spectral split.” In a two-flavor language, it is explained as follows. The strong neutrino-neutrino interactions lead to a synchronization of the neutrino oscillations. The flavor polarization vector of the ensemble begins at high density essentially aligned with the ν_e direction in flavor space. After passing the MSW region, the polarization vector emerges with a significant transverse component relative to the mass direction because the MSW transition is not fully adiabatic. Subsequently this MSW-prepared initial condition is subject to collective effects only. As the effective neutrino-neutrino interaction be-

comes weaker, the modes above a certain energy E_{split} orient themselves along the mass direction, those with smaller energies in the opposite direction. This is precisely the “neutrino only” case studied in Refs. [28, 29] as a generic case for a spectral split, a case that requires one to prepare the polarization vector with a large transverse component. (For neutrinos plus antineutrinos, the MSW preparation is not necessary because the collective pair transformations alone engineer a split.)

Our main goal here is to use the picture of a MSW-prepared spectral split to derive analytically the main features seen in Duan et al.’s numerical study [34], viz. the existence and the positions of the spectral splits.

The numerical model in Fig. 1 shows that the MSW resonances are within the collective neutrino region, but not deeply inside. Therefore it is not a priori obvious if the “synchronized MSW preparation” and the subsequent “split” can be clearly separated. For our discussion we therefore adopt a more schematic model. We artificially increase the neutrino-neutrino interaction strength (raise the μ -profile in Fig. 1) such that the MSW region and the spectral split regions are clearly separate. In this framework we first calculate the MSW preparation analytically and then study a three-flavor treatment of the spectral split, based on the machinery recently developed by two of us [36]. We find that our analytic treatment reproduces the numerical results surprisingly well. It also reproduces all relevant features of the realistic case, i.e. with the μ -profile of Fig. 1, justifying our simplifying assumptions and verifying our general interpretation.

We first set up in Sec. II our schematic SN model that captures the features relevant for our treatment and continue in Sec. III with the equations of motion. In Sec. IV we derive analytically the MSW-prepared three-flavor state that serves as input for our three-flavor spectral split study in Sec. V. We conclude in Sec. VI.

II. SIMPLIFIED SUPERNOVA MODEL

A. Realistic scenario

We take the electron density profile n_e obtained from numerical studies of O-Ne-Mg core SNe [39, 40, 41], providing $\lambda(r)$ as shown in our Fig. 1. The neutrino luminosity is assumed to be $L_{\nu_e} = 10^{53}$ erg s $^{-1}$ with a Fermi-Dirac spectrum with the average energy $\langle E_{\nu_e} \rangle = 11$ MeV and a degeneracy parameter $\eta = 3$, implying a temperature $T = 2.76$ MeV. The neutrino sphere is taken at the radius $R = 60$ km, implying an effective neutrino-neutrino interaction strength at large distances of

$$\mu(r) = \mu_0 \left(\frac{\text{km}}{r} \right)^4 \quad (1)$$

with $\mu_0 = 8.6 \times 10^{11}$ km $^{-1}$. This is the profile shown in Fig. 1. Based on this model we have solved the equations of motion numerically and found the electron neutrino

survival probability shown in Fig. 2, in agreement with the results of Duan et al. [34].

In this realistic situation, the decrease of the effective neutrino-neutrino interaction with radius is such that the spectral split is essentially adiabatic. Quantitatively, the length scale $\ell_\mu \equiv |d \ln \mu(r)/dr|^{-1}$ is large enough to satisfy the adiabaticity condition (see Sec. V of [28]) during the spectral split. The very development of a step-like feature in P_{ee} in Fig. 2 is an expression of the adiabaticity. The “sharpness” of the step in P_{ee} is a measure of the degree of adiabaticity, an extremely slowly decreasing neutrino-neutrino interaction corresponds to a perfect step function in P_{ee} [28, 29].

B. Analytical treatment

Our analytic treatment is based on a schematic representation of the essentials of this realistic case. We picture that the synchronized MSW effect occurs first and factorizes from the collective oscillations that lead to the spectral split. To this end, we consider the limiting case where μ_0 in eq. (1) is arbitrarily large. This makes the H and L level crossings more synchronized, and pushes the regions where the spectral splits occur, i.e. the regions where $\mu(r)$ becomes comparable to ω_H or ω_L , to much larger radii. This also renders the spectral splits even more adiabatic¹, making the steps in P_{ee} sharper.

It is also important that the MSW transition is not perfectly adiabatic. In our schematic model, we use the power-law profile for the matter potential,

$$\lambda(r) = \lambda_0 \left(\frac{r_0}{r} \right)^a \quad (2)$$

with $\lambda_0 = 10^3$ km $^{-1}$, $r_0 = 900$ km and $a = 50$. This approximates reasonably the numerical $\lambda(r)$ profile of Fig. 1 in the neighborhood of the H and L crossings. This allows an analytic estimate of the level crossing probabilities at the two resonances.

Thus, we obtain our analytic results in the limit of $\mu_0 \rightarrow \infty$ and a power law profile for $\lambda(r)$, where (i) the MSW transitions are perfectly synchronized but semia-
diabatic, (ii) the spectral split regions are well separated from the MSW region, and (iii) the spectral splits are perfectly adiabatic, making the steps in P_{ee} infinitely sharp. Apart from these minor changes, the physical pictures with the realistic profile and our schematic profile are identical.

¹ Since $\mu(r)$ is a power law, the length scale ℓ_μ increases with increasing r . As a result, larger radius for spectral split implies larger ℓ_μ and more adiabaticity

C. Numerical treatment

We also study the spectral splits numerically, assuming the analytic MSW-prepared spectra as input. For such a numerical illustration we employ

$$\mu_0 = 10^{15} \text{ km}^{-1}, \quad (3)$$

much larger than the realistic value shown in Fig. 1.

The analytic results match the numerical ones in all details, and reproduce the main features of the realistic situation, with a minor difference that the spectral splits appear sharper. This is because the net effect of our approximations is only to make the MSW resonances more synchronized, and the spectral splits more adiabatic.

III. EQUATIONS OF MOTION

A. Matrices of density

Mixed neutrinos are described by matrices of density $\varrho_{\mathbf{p}}$ for each momentum. The diagonal entries are the usual occupation numbers whereas the off-diagonal terms encode phase information. The equations of motion (EOMs) are

$$i d_t \varrho_{\mathbf{p}} = [\mathbf{H}_{\mathbf{p}}, \varrho_{\mathbf{p}}], \quad (4)$$

where the Hamiltonian is [12]

$$\mathbf{H}_{\mathbf{p}} = \Omega_{\mathbf{p}} + \mathbf{V} + \sqrt{2} G_{\text{F}} \int \frac{d^3 \mathbf{q}}{(2\pi)^3} (\varrho_{\mathbf{q}} - \bar{\varrho}_{\mathbf{q}}) (1 - \mathbf{v}_{\mathbf{q}} \cdot \mathbf{v}_{\mathbf{p}}), \quad (5)$$

$\mathbf{v}_{\mathbf{p}}$ being the velocity. The matrix of vacuum oscillation frequencies is $\Omega_{\mathbf{p}} = \text{diag}(m_1^2, m_2^2, m_3^2)/2|\mathbf{p}|$ in the mass basis. The matter effect is represented, in the weak interaction basis, by $\mathbf{V} = \sqrt{2} G_{\text{F}} n_e \text{diag}(1, 0, 0)$. While in general there is a second-order difference between the ν_{μ} and ν_{τ} refractive index [43] that can be important for collective neutrino oscillations [35], for the low matter densities relevant in our case this ‘‘mu-tau matter term’’ is irrelevant.

The factor $(1 - \mathbf{v}_{\mathbf{q}} \cdot \mathbf{v}_{\mathbf{p}})$ in $\mathbf{H}_{\mathbf{p}}$ implies ‘‘multi-angle effects’’ for neutrinos moving on different trajectories [21, 22, 24]. However, for realistic SN conditions the modifications are small, allowing for a single-angle approximation [24, 30]. In the strongly synchronized regime this is not surprising: the strong neutrino-neutrino interaction causes self-maintained coherence not only between different energy modes, but also between different angular modes. It has not been explained why the single-angle approximation remains good even when the neutrino-neutrino interaction becomes weak, although numerically this is observed to be the case [24, 30, 33].

We are studying the spatial evolution of the neutrino fluxes in a quasi-stationary situation. Therefore, the matrices $\varrho_{\mathbf{p}}$ do not depend on time explicitly so that the total time derivative in the EOMs reduces to the Liouville

term involving only spatial derivatives. (See Ref. [44] for a recent comprehensive discussion of the role of the Liouville term in Boltzmann collision equations involving oscillating neutrinos.) Moreover, we consider a spherically symmetric system so that the only spatial variable is the radial coordinate r . In the single-angle approximation we finally need to study the simple EOMs,

$$i \partial_r \varrho_{\omega} = [\mathbf{H}_{\omega}, \varrho_{\omega}], \quad (6)$$

where we now classify different modes by the variable

$$\omega = \frac{\Delta m_{\text{atm}}^2}{2E}. \quad (7)$$

The single-mode Hamiltonians are

$$\mathbf{H}_{\omega} = \Omega_{\omega} + \lambda(r) \mathbf{L} + \mu(r) \varrho. \quad (8)$$

Here we have introduced $\lambda(r) = \sqrt{2} G_{\text{F}} n_e(r)$ and $\mathbf{L} = \text{diag}(1, 0, 0)$ in the weak interaction basis. The matrix of the total density $\varrho = \int d\omega \varrho_{\omega}$ is normalized such that at the neutrino sphere it is $\varrho = \text{diag}(1, 0, 0)$ in the weak interaction basis. It is conserved except for oscillation effects, i.e., the physical neutrino density has been absorbed in the coefficient $\mu(r)$ that measures a suitable angular average of the neutrino-neutrino interaction energy. The radial variation is $\mu(r) \propto r^{-4}$ where a factor r^{-2} comes from the geometric flux dilution, another approximate factor r^{-2} from the fact that neutrinos become more collinear with distance from the source.

B. Mixing parameters

Since \mathbf{H}_{ω} appears in a commutator we may arbitrarily add terms proportional to the 3×3 unit matrix. It will prove convenient to express the matrix of vacuum oscillation frequencies in the form

$$\Omega_{\omega} = \omega \text{diag} \left(-\frac{1}{2}\alpha, +\frac{1}{2}\alpha, \pm 1 \right), \quad (9)$$

where the mass hierarchy parameter is

$$\alpha \equiv \frac{\Delta m_{\odot}^2}{\Delta m_{\text{atm}}^2} \approx \frac{1}{30}. \quad (10)$$

A positive sign in the third component of Ω_{ω} signifies the normal mass hierarchy, a negative sign the inverted hierarchy. For the mass differences themselves we use [45]

$$\begin{aligned} \Delta m_{\text{atm}}^2 &= 2.4 \times 10^{-3} \text{ eV}^2, \\ \Delta m_{\odot}^2 &= 8 \times 10^{-5} \text{ eV}^2. \end{aligned} \quad (11)$$

For the mixing angles we use

$$\begin{aligned} \theta_{12} &= 0.6, \\ \theta_{23} &= \pi/4, \\ \theta_{13} &= 0.1. \end{aligned} \quad (12)$$

Of course, for θ_{13} only upper limits exist. In this context the CP phase δ_{CP} can be ignored, since it does not influence the relevant probabilities for equal ν_{μ} and ν_{τ} fluxes [46, 47].

C. Bloch vectors

In the two-flavor context it is well known that the matrices of density can be expressed in terms of Bloch vectors, leading to EOMs that resemble the precession of a gyroscope around an external force field. This picture helps to recognize properties of the EOMs that are difficult to fathom in the commutator form of the EOMs. Therefore, we follow a recent paper by two of us [36] and note that every Hermitean 3×3 matrix \mathbf{X} can be expressed in the form

$$\mathbf{X} = \frac{1}{3} X_0 + \frac{1}{2} \mathbf{X} \cdot \mathbf{\Lambda}, \quad (13)$$

where $X_0 = \text{Tr}(\mathbf{X})$, \mathbf{X} is an eight-dimensional Bloch vector, and $\mathbf{\Lambda}$ is a vector of the Gell-Mann matrices. Note that $\Lambda_3 = \text{diag}(1, -1, 0)$ and $\Lambda_8 = \text{diag}(1, 1, -2)/\sqrt{3}$.

The Bloch vector for the single-mode Hamiltonian is \mathbf{H}_ω whereas the one for ϱ_ω is the polarization vector \mathbf{P}_ω . Then the single-mode EOMs are

$$\dot{\mathbf{P}}_\omega = \mathbf{H}_\omega \times \mathbf{P}_\omega, \quad (14)$$

where the cross product is understood in the SU(3) sense: $(\mathbf{A} \times \mathbf{B})_i = f_{ijk} A_j B_k$ where $i, j, k = 1, \dots, 8$ and f_{ijk} are the structure constants of the SU(3) Lie algebra.

With the global polarization vector $\mathbf{P} = \int d\omega \mathbf{P}_\omega$ and ignoring the ordinary matter term, we write the single-mode Hamiltonian in the form

$$\mathbf{H}_\omega = \omega (\mathbf{B}_H + \alpha \mathbf{B}_L) + \mu \mathbf{P}. \quad (15)$$

In the mass basis, the ‘‘magnetic field’’ components are

$$\mathbf{B}_H = -\frac{2}{\sqrt{3}} \mathbf{e}_8 \quad \text{and} \quad \mathbf{B}_L = -\mathbf{e}_3, \quad (16)$$

representing the ‘‘atmospheric’’ and ‘‘solar mass directions,’’ respectively.

In the absence of ordinary matter, the EOM for the global polarization vector is

$$\dot{\mathbf{P}} = (\mathbf{B}_H + \alpha \mathbf{B}_L) \times \mathbf{M}, \quad (17)$$

where the ‘‘magnetic moment’’ of the system is $\mathbf{M} = \int d\omega \omega \mathbf{P}_\omega$. In the mass basis this is

$$\dot{\mathbf{P}} = -\left(\frac{2}{\sqrt{3}} \mathbf{e}_8 + \alpha \mathbf{e}_3\right) \times \mathbf{M}. \quad (18)$$

The vector on the r.h.s. is orthogonal to both \mathbf{e}_3 and \mathbf{e}_8 . The reason is that the matrices Λ_3 and Λ_8 commute or, in other words, that $f_{a38} = 0$ for $a = 1, \dots, 8$ and the same for all permutations. As a consequence, the vector $\dot{\mathbf{P}}$ has no \mathbf{e}_3 or \mathbf{e}_8 component so that $\dot{P}_3 = 0$ and $\dot{P}_8 = 0$. In a general basis this implies

$$d_t(\mathbf{P} \cdot \mathbf{B}_H) = 0 \quad \text{and} \quad d_t(\mathbf{P} \cdot \mathbf{B}_L) = 0. \quad (19)$$

This is the equivalent of ‘‘flavor-lepton number conservation’’ $d_t(\mathbf{P} \cdot \mathbf{B}) = 0$ in the two-flavor context [25, 28, 29].

In other words, in the three-flavor context we have two flavor-lepton numbers that are separately conserved. In the mass basis one concludes that

$$\begin{aligned} P_3 &= \varrho_{11} - \varrho_{22}, \\ P_8 &= \frac{\varrho_{11} + \varrho_{22} - 2\varrho_{33}}{\sqrt{3}} \end{aligned} \quad (20)$$

are conserved.

IV. SYNCHRONIZED MSW EFFECT

As a first step in our analytic study we consider the matter-induced conversion of the initial ν_e flux as it passes the H and L level crossings, assuming that both lie deeply in the region where the neutrino-neutrino interaction is strong. As a result, the flavor oscillations are synchronized, meaning that all ϱ_ω stay pinned to each other. In other words, it is enough to study the evolution of the matrix of the total density ϱ . It obeys the EOM

$$i\partial_r \varrho(r) = [\Omega + \lambda(r)L, \varrho(r)], \quad (21)$$

where in the mass basis

$$\Omega = \omega_0 \text{diag}\left(-\frac{1}{2}\alpha, +\frac{1}{2}\alpha, \pm 1\right) \quad (22)$$

and $\omega_0 = \langle \Delta m_{\text{atm}}^2 / 2E \rangle$.

For the Fermi-Dirac spectrum described in Sec. II we find $\omega_0 = 0.710 \text{ km}^{-1}$. We will also use the notation

$$\begin{aligned} \omega_H &= \left\langle \frac{\Delta m_{\text{atm}}^2}{2E} \right\rangle = \omega_0 = 0.710 \text{ km}^{-1}, \\ \omega_L &= \left\langle \frac{\Delta m_{\odot}^2}{2E} \right\rangle = \alpha \omega_0 = 0.024 \text{ km}^{-1}. \end{aligned} \quad (23)$$

The matrix of vacuum oscillation frequencies thus can also be written as $\Omega = \text{diag}\left(-\frac{1}{2}\omega_L, +\frac{1}{2}\omega_L, \pm\omega_H\right)$.

The assumed perfect synchronization implies that we can treat this system as an equivalent system with a single energy² or rather with two fixed vacuum frequencies ω_H and ω_L determining Ω . It is most useful to study its evolution in the basis of instantaneous propagation eigenstates where we denote the total matrix of density as $\tilde{\varrho}$. Since the only effect of the neutrino-neutrino interactions is to synchronize the oscillations and to reduce the system to an equivalent single-energy case, the propagation eigenstates are defined by the ordinary matter term for a monochromatic neutrino beam, whereas the neutrino-neutrino interaction plays no further role. The propagation basis coincides with the weak interaction basis when

² An MSW transition in the presence of a dense neutrino gas was first treated in this way in the context of early-universe neutrino oscillations by Wong [18] and by Abazajian, Beacom and Bell [19]. They used the terminology ‘‘collective MSW-like transformation’’ and ‘‘synchronized MSW effect,’’ respectively.

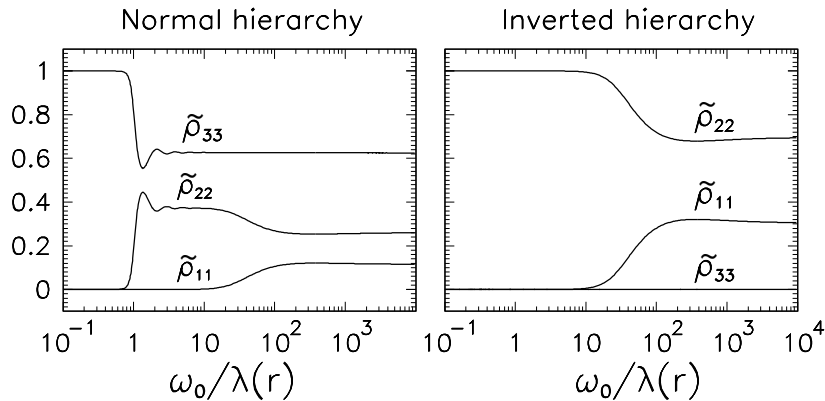


FIG. 3: Evolution of the diagonal elements of the matrix of densities $\tilde{\rho}_\omega$ for a mode with $\omega = 0.42 \text{ km}^{-1}$, represented in the basis of instantaneous propagation eigenstates. Due to the synchronization, all modes behave similarly.

TABLE I: Final occupations of the mass eigenstates after passing both MSW level crossings as described in the text.

	Normal hierarchy		Inverted hierarchy	
$\tilde{\rho}_{11}$	$P_H P_L$	0.12	P_L	0.31
$\tilde{\rho}_{22}$	$P_H (1 - P_L)$	0.26	$(1 - P_L)$	0.69
$\tilde{\rho}_{33}$	$(1 - P_H)$	0.62	0	0

the matter density is large so that our initial state is $\tilde{\rho} = \text{diag}(0, 0, 1)$ in normal hierarchy, and $\text{diag}(0, 1, 0)$ in inverted hierarchy. If the subsequent evolution were perfectly adiabatic, the system would remain in this state so that the ν_e survival probability after the H and L crossings would be given by well known results [1].

We assume indeed that the evolution is adiabatic, except near the H and L level crossings where in our system the jumping probabilities P_H and P_L need not be small. The neutrino mass-gap hierarchy ensures that the two crossings factorize with good approximation. In the normal hierarchy, the system encounters both crossings and the final occupation of the propagation eigenstates is given by the products of probabilities shown in Table I. In the inverted hierarchy, only the L crossing is encountered because the H level crossing is now in the antineutrino sector that is irrelevant in our case. Again, the final mass-state occupations are shown in Table I.

The jumping probability for incomplete adiabaticity is given to a good approximation by the so-called double-exponential formula [48, 49, 50]

$$P_H = \frac{\exp(2\pi R_H \omega_H \cos^2 \theta_{13}) - 1}{\exp(2\pi R_H \omega_H) - 1}, \quad (24)$$

where the scale height is

$$R_H = \left| \frac{d \ln \lambda(r)}{dr} \right|_{r=r_H}^{-1}. \quad (25)$$

It has to be evaluated at the point of maximum violation of adiabaticity [51, 52, 53], given by $\omega_H = \lambda(r_H)$ [50]. The

assumed power-law profile of Eq. (2) and our choices for ω_H and θ_{13} imply $r_H = 1089 \text{ km}$, $R_H = 21.8 \text{ km}$, and $P_H = 0.38$. Analogous results pertain to P_L with $H \rightarrow L$ everywhere and the substitution $\theta_{13} \rightarrow \theta_{12}$. We find $r_L = 1166 \text{ km}$, $R_L = 23.3 \text{ km}$, and $P_L = 0.31$. These numerical results for P_H and P_L imply the numerical results for the final occupations shown in Table I.

In the steep density profile used here, the H and L resonances look spatially very close (Fig. 1) so that one may worry if they indeed factorize in the usual way. We stress that the two resonances do not overlap, but one may still worry about possible interference effects. However, we can compare the analytic results with a numerical three-flavor evolution, using the same power-law $\lambda(r)$ profile. In Fig. 3 we show the evolution of the diagonal elements of $\tilde{\rho}_\omega$, for a mode with $\omega = 0.42 \text{ km}^{-1}$, as a function of $\omega_0/\lambda(r)$. Due to the synchronization condition, all frequency modes behave the same. On this scale, the H crossing is at $\omega_0/\lambda(r) = 1$ and the L crossing at $\omega_0/\lambda(r) = \alpha^{-1} = 30$. The agreement between the numerical end states and the analytically predicted ones is striking.

V. SPECTRAL SPLIT

After the system has passed the two MSW level crossings, the ordinary matter density quickly becomes negligible, whereas by assumption the neutrino-neutrino effects are still strong. The subsequent evolution to the point where the neutrino-neutrino interaction becomes negligible will then produce spectral splits in the same way as described in Refs. [28, 29]. We can follow the previous two-flavor treatment almost step by step because the present three-flavor system is simplified by the mass-gap hierarchy $\alpha \approx 1/30 \ll 1$. While the two conserved flavor-lepton numbers present in the three flavor case lead to two spectral splits, these will occur in sequence and their dynamics factorizes in practice.

The first split to develop is driven by the atmospheric

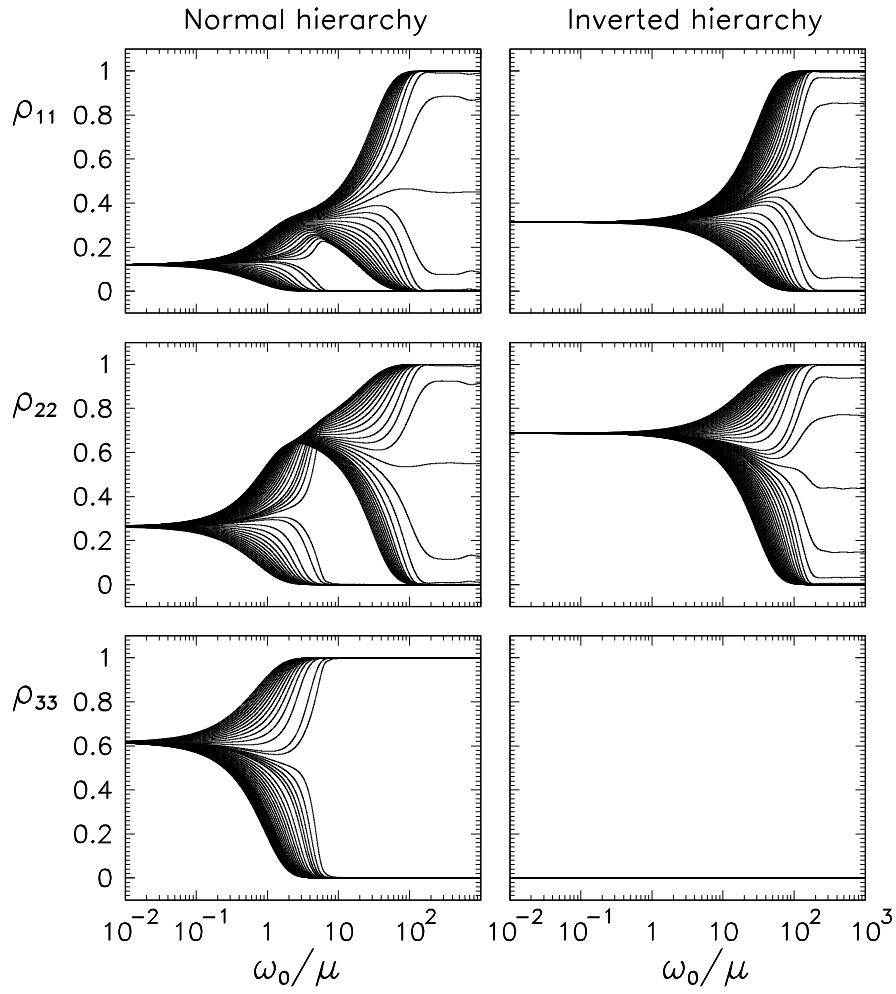


FIG. 4: Evolution of the diagonal elements of ϱ_ω for our box-spectrum example. The mode density is increased around the splits.

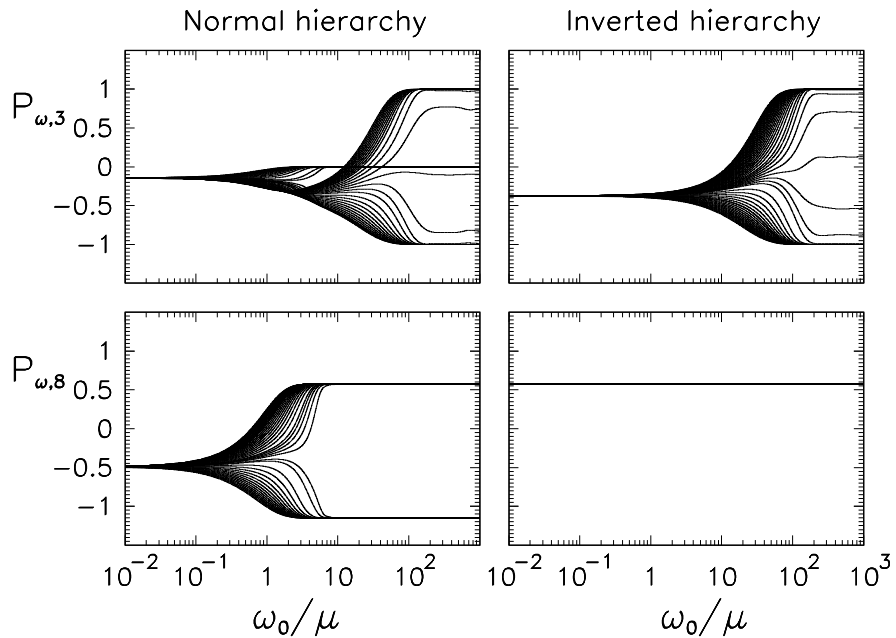


FIG. 5: Evolution of the 3 and 8 components of \mathbf{P}_ω for our box-spectrum example.

mass difference and thus can be called the H split. As in Refs. [28, 29] we go to a rotating frame, at first rotating around the \mathbf{B}_H direction. The single-mode Hamiltonians in this co-rotating frame are

$$\mathbf{H}_\omega \approx (\omega - \omega_H^c) \mathbf{B}_H + \mu \mathbf{P}, \quad (26)$$

neglecting for now the much smaller term $\alpha\omega\mathbf{B}_L$. This is justified because, when $\mu \gtrsim \omega$ (and thus $\mu \gg \alpha\omega$), the ensemble of neutrinos is in a regime where we expect spectral splitting along \mathbf{e}_8 and synchronized oscillations along \mathbf{e}_3 . This factorization has been explicitly shown in [36]. Flavor conversion is thus driven primarily by \mathbf{B}_H , while \mathbf{B}_L gives sub-leading corrections due to the synchronized oscillations. Similarly, when $\mu \sim \alpha\omega$, flavor conversion proceeds efficiently via a spectral split along \mathbf{e}_3 and is driven by \mathbf{B}_L , while \mathbf{B}_H drives vacuum oscillations along \mathbf{e}_8 .

Now, as μ adiabatically goes to zero, the co-rotation frequency ω_H^c approaches the final split frequency ω_H^s and the modes with $\omega > \omega_H^s$ will orient themselves along \mathbf{B}_H , those with $\omega < \omega_H^s$ in the $-\mathbf{B}_H$ direction. The value of ω_H^s is fixed by the conservation of P_8 . Since the evolution associated with \mathbf{B}_H has saturated, we can next go into a frame rotating around \mathbf{B}_L where

$$\mathbf{H}_\omega \approx (\omega - \omega_L^c) \mathbf{B}_L + \mu \mathbf{P} \quad (27)$$

and repeat the analogous argument.

To illustrate the dynamics of the split in a form similar to Refs. [28, 29] we consider an explicit example with an initial ‘‘box spectrum’’ at high density of the form

$$\varrho_{ee}(\omega) = \begin{cases} (2\omega_0)^{-1} & \text{for } 0 \leq \omega \leq 2\omega_0, \\ 0 & \text{otherwise.} \end{cases} \quad (28)$$

At high densities $\rho_{ee}(\omega)$ coincides with $\tilde{\rho}_{33}(\omega)$ in normal hierarchy and with $\tilde{\rho}_{22}(\omega)$ in inverted hierarchy. After the MSW crossings the spectrum is still of box shape because of the assumed strong neutrino-neutrino interaction, but now has the ϱ_{11} , ϱ_{22} , and ϱ_{33} components shown in Table I. Note that after the MSW transitions we neglect ordinary matter so that the propagation eigenstates are identical with the mass eigenstates and $\tilde{\varrho} = \varrho$.

A. Normal hierarchy

At first we study the evolution caused by the neutrino-neutrino interactions numerically. To this end we use the usual $\mu(r) \propto r^{-4}$ profile of Eq. (1) with the coefficient μ_0 of Eq. (3). In this way the evolution is strongly but not perfectly adiabatic. Of course, the analytic results, based on the conservation of flavor-lepton number, apply in the perfectly adiabatic limit which here requires $\mu_0 \rightarrow \infty$.

In Fig. 4 (left column) we show the evolution in the mass basis of the diagonal elements of ρ_ω for 50 modes as a function of ω_0/μ . All modes start with the same initial condition prepared by the MSW transitions. Around $\omega_0/\mu = 1$ one recognizes a first H split that affects all

components. Around $\omega_0/\mu = \alpha^{-1}$ one recognizes a second split, the L split, that affects only ρ_{11} and ρ_{22} . During the H split, the modes with $\omega < \omega_H^s$ tend to $\rho_{33} \rightarrow 0$, while those with $\omega > \omega_H^s$ approach $\rho_{33} \rightarrow 1$. Then ρ_{11} and ρ_{22} modes with $\omega > \omega_H^s$ go to 0, as implied by the conservation of the trace of ρ . While the modes with $\omega < \omega_H^s$ rise towards higher values of ρ_{11} and ρ_{22} , they encounter the L split at a frequency $\omega_L^s < \omega_H^s$. At this split, for $\omega < \omega_L^s$, the ρ_{11} approach 1 and the ρ_{22} approach 0, and vice versa for $\omega_L^s < \omega < \omega_H^s$. As a result of imperfect adiabaticity some modes do not reach these extreme values, but get frozen earlier.

In Fig. 5 (left column) we show the same case in terms of the mass-basis $P_{\omega,3}$ and $P_{\omega,8}$ components. We observe that in $P_{\omega,8}$ only the H split operates whereas in $P_{\omega,3}$ the H and L splits operate in sequence.

The situation can be visualized in terms of the \mathbf{e}_3 – \mathbf{e}_8 triangle diagram [36] shown in Fig. 6. Each point in the interior and on the boundary of the triangle represents the projection of the polarization vector \mathbf{P}_ω in the \mathbf{e}_3 – \mathbf{e}_8 plane. Neutrinos from the ν_e burst start in the state $\nu_e \approx \tilde{\nu}_3$, where by ‘‘tilde’’, we represent the instantaneous mass eigenstates. The H crossing shifts the neutrino state from the $\tilde{\nu}_3$ vertex towards the $\tilde{\nu}_2$ state, but only partially, due to the semiadiabatic nature of the transition. After that crossing, all neutrinos find themselves at the point A' inside the triangle. The L crossing further transports the state along a line parallel to the $\tilde{\nu}_2$ – $\tilde{\nu}_1$ edge towards $\tilde{\nu}_1$, again only partly due to the semiadiabaticity. Before the split, all the neutrinos are thus at a point A in the interior of the triangle.

The H split takes the $\omega > \omega_H^s$ modes towards the $\tilde{\nu}_3$ state ($P_{\omega,3} = 0, P_{\omega,8} = -2/\sqrt{3}$) and the modes $\omega < \omega_H^s$ towards some combination of $\tilde{\nu}_1$ and $\tilde{\nu}_2$, while conserving the total P_3 and P_8 . Since $\alpha \ll 1$, the H and L splits are well separated and the high- ω modes reach the $\tilde{\nu}_3$ vertex, i.e. the H split saturates, before the L split begins. The low- ω modes propagating towards the $P_{\omega,8} = 1/\sqrt{3}$ line encounter the L split that tends to take the $\omega > \omega_L^s$ modes towards $\tilde{\nu}_2$ ($P_{\omega,3} = -1, P_{\omega,8} = 1/\sqrt{3}$) and the $\omega < \omega_L^s$ modes towards $\tilde{\nu}_1$ ($P_{\omega,3} = 1, P_{\omega,8} = 1/\sqrt{3}$). In the adiabatic limit, given sufficient time to propagate, the H and L splits result in all neutrinos reaching one of the three vertices of the \mathbf{e}_3 – \mathbf{e}_8 triangle.

Using the conservation law for P_3 and P_8 of Eq. (20) one can evaluate the split frequencies ω_H^s and ω_L^s . For $\omega < \omega_H^s$ we have $P_{\omega,8} \rightarrow 1/\sqrt{3}$, while for $\omega > \omega_H^s$ they reach $-2/\sqrt{3}$. In the limit of perfect adiabaticity, the conservation of P_8 implies

$$2\omega_0 P_{\omega,8}^0 = \frac{1}{\sqrt{3}} \omega_H^s - \frac{2}{\sqrt{3}} (2\omega_0 - \omega_H^s), \quad (29)$$

where $P_{\omega,8}^0$ is the common value of $P_{\omega,8}$ before the split begins. In our example, $P_{\omega,8}^0 = -0.50$, leading to $\omega_H^s = 0.76\omega_0$.

When the H split saturates, all modes with $\omega > \omega_H^s$ have $P_{\omega,8} = -2/\sqrt{3}$, and hence $P_{\omega,3} = 0$ due to the

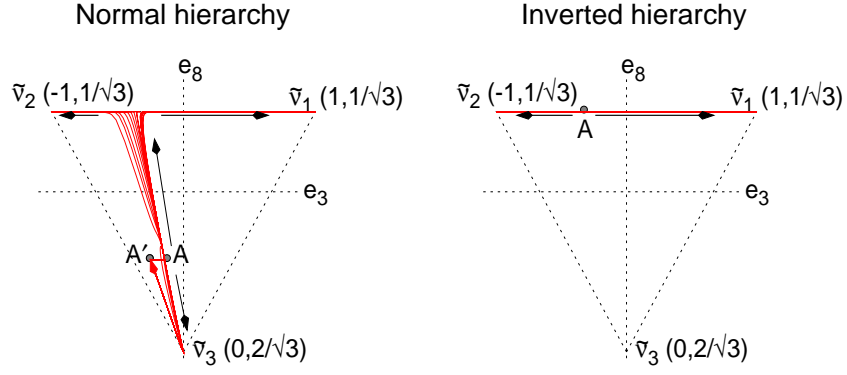


FIG. 6: Projection of the polarization vectors \mathbf{P}_ω on the e_3 - e_8 plane for our box-example. The vertices of the triangle represent pure (instantaneous) mass eigenstates. After both MSW transitions, the system is at the point A in the interior of the triangle. (See the text for details.)

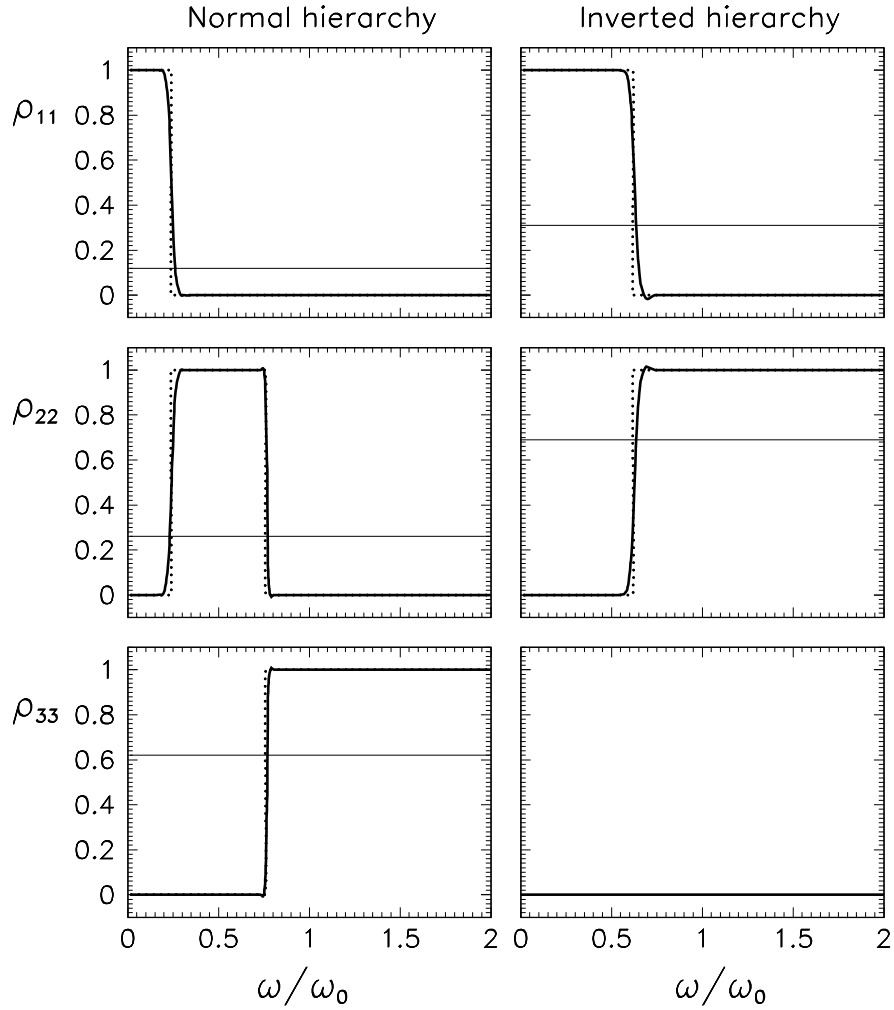


FIG. 7: Diagonal elements of ϱ_ω . Thin line: initial box spectrum. Thick line: final numerical spectrum. Dotted line: final spectrum in the adiabatic limit.

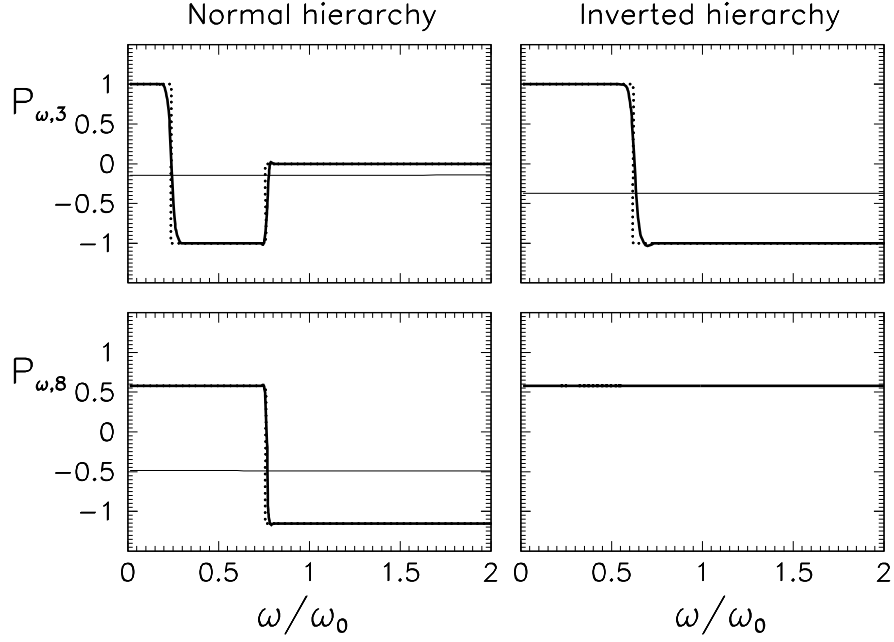


FIG. 8: The 3 and 8 components of \mathbf{P}_ω . Convention for lines is same as in Fig. 7.

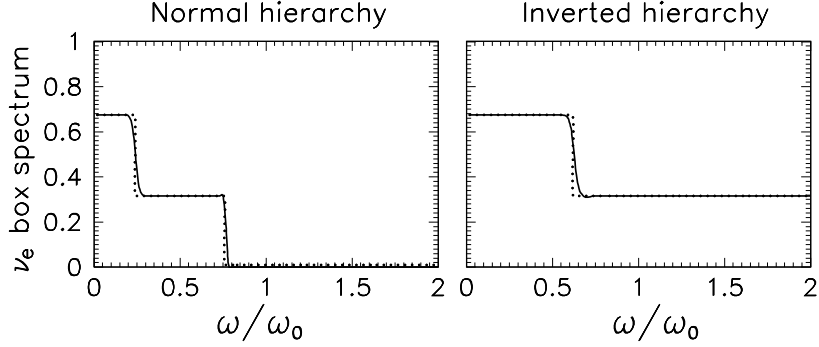


FIG. 9: The ν_e component at a large distance so that the different ω modes have kinematically decohered. Convention for lines is same as in Fig. 7.

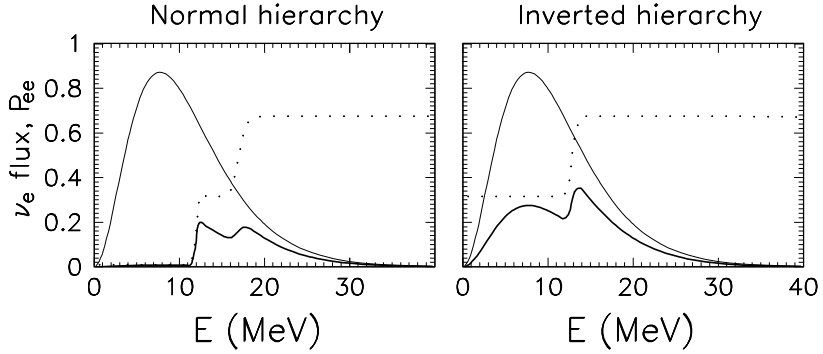


FIG. 10: Initial (thin) and final (thick) spectrum for a Fermi-Dirac distribution with the parameters described in Sec. II. The numerical final spectrum is for our toy-model SN where the MSW crossings and spectral-split region are far separated. Dotted curves represent the survival probability P_{ee} for electron neutrinos.

conservation of the norm of \mathbf{P} . These modes have reached the bottom vertex of the \mathbf{e}_3 - \mathbf{e}_8 triangle and hence cannot split further due to the L split. On the other hand, for modes with $\omega < \omega_{\text{H}}^{\text{s}}$ a second split in $P_{\omega,3}$ happens. These modes approach $P_{\omega,3} = +1$ for $\omega < \omega_{\text{L}}^{\text{s}}$ and $P_{\omega,3} = -1$ for $\omega > \omega_{\text{L}}^{\text{s}}$. Applying the conservation law for P_3 gives us

$$2\omega_0 P_{\omega,3}^0 = \omega_{\text{L}}^{\text{s}} - (\omega_{\text{H}}^{\text{s}} - \omega_{\text{L}}^{\text{s}}). \quad (30)$$

In our example $P_{\omega,3}^0 = -0.14$ so that $\omega_{\text{L}}^{\text{s}} = 0.24\omega_0$.

We show in Figs. 7 and 8 the mass-basis spectra of the diagonal elements of ϱ and of P_3 and P_8 . Thin lines are the MSW-prepared initial spectra. Thick lines show the numerical end states, corresponding to the split diagrams of Figs. 4 and 5. Dotted lines show the adiabatic limiting behavior based on the lepton-number conservation laws. Once more the agreement is striking. Imperfect adiabaticity leads to a smoothening of the splits which otherwise are sharp spectral steps.

Finally, in Fig. 9 we show the ν_e spectrum after the two splits. The solid curve is the numerical result, where the vacuum oscillations between the SN and the observer have been averaged (kinematical decoherence between different ω modes), i.e.,

$$\varrho_{ee} = U_{e1}^2 \varrho_{11} + U_{e2}^2 \varrho_{22} + U_{e3}^2 \rho_{33}. \quad (31)$$

The dotted curve is our analytic result in the adiabatic limit. This result is easily explained if we observe that in Eq. (31) in the case of maximal 23 mixing one has $U_{e1}^2 = \cos^2 \theta_{13} \cos^2 \theta_{12}$, $U_{e2}^2 = \cos^2 \theta_{13} \sin^2 \theta_{12}$, and $U_{e3}^2 = \sin^2 \theta_{13}$. Therefore,

$$\rho_{ee} \simeq \begin{cases} \cos^2 \theta_{12} & \text{for } \omega < \omega_{\text{L}}^{\text{s}}, \\ \sin^2 \theta_{12} & \text{for } \omega_{\text{L}}^{\text{s}} < \omega < \omega_{\text{H}}^{\text{s}}, \\ \sin^2 \theta_{13} & \text{for } \omega_{\text{H}}^{\text{s}} < \omega. \end{cases} \quad (32)$$

Again the agreement between the analytic and numerical results is very good.

B. Inverted hierarchy

For the inverted hierarchy we show the analogous information in the right-handed columns of Figs. 4–9. The initial state here is $\tilde{\nu}_2$. The nonadiabatic L crossing takes the neutrino states partly towards $\tilde{\nu}_1$. After the L crossing and before the split, the neutrino state for all modes is along the $\tilde{\nu}_1$ - $\tilde{\nu}_2$ edge, at A as shown in Fig. 6 (right column), where $P_{\omega,8} = 1/\sqrt{3}$. Since all neutrinos already are in one of the extreme values of $P_{\omega,8}$, the H split is inoperational. This corresponds to ρ_{33} remaining in its MSW-prepared initial value of 0. The L split takes $\rho_{11} \rightarrow +1$ for $\omega < \omega_{\text{L}}^{\text{s}}$ and $\rho_{11} \rightarrow 0$ for $\omega > \omega_{\text{L}}^{\text{s}}$, and vice versa for ρ_{22} . In the inverted hierarchy we have an effective two-flavor case in the ν_1 - ν_2 subsector. This is a consequence of the MSW-prepared initial condition. Initially $P_{\omega,8}^0 = 1/\sqrt{3}$. Applying now the conservation of P_8 we obtain $\omega_{\text{H}}^{\text{s}} = 2\omega_0$, i.e., the split occurs at the edge

of the box and thus is not visible. The conservation law for P_3 and using in our case $P_{\omega,3}^0 = -0.38$, one obtains $\omega_{\text{L}}^{\text{s}} = 0.62\omega_0$. For the electron flavor we predict for the final spectrum

$$\rho_{ee} \simeq \begin{cases} \cos^2 \theta_{12} & \text{for } \omega < \omega_{\text{L}}^{\text{s}}, \\ \sin^2 \theta_{12} & \text{for } \omega_{\text{L}}^{\text{s}} < \omega, \end{cases} \quad (33)$$

in agreement with the numerical result.

Note that in the inverted hierarchy, there is only one split. This is because $P_{\omega,8}$ is already at an extreme value before the split can begin. In general, there are two splits if the neutrino state before the split is in the interior of the \mathbf{e}_3 - \mathbf{e}_8 triangle, one split if it is along one of the edges of the triangle (as in this case), and no split occurs if the neutrino state is at any of the three vertices (See Fig. 6).

C. Fermi-Dirac spectrum

It is straightforward to extend these arguments to a general spectrum, e.g. a Fermi-Dirac spectrum $f(\omega)$. The conservation laws imply for the normal hierarchy

$$\begin{aligned} \sqrt{3}P_{\omega,8}^0 &= \int_0^{\omega_{\text{H}}^{\text{s}}} d\omega f(\omega) - 2 \int_{\omega_{\text{H}}^{\text{s}}}^{\infty} d\omega f(\omega), \\ P_{\omega,3}^0 &= \int_0^{\omega_{\text{L}}^{\text{s}}} d\omega f(\omega) - \int_{\omega_{\text{L}}^{\text{s}}}^{\omega_{\text{H}}^{\text{s}}} d\omega f(\omega). \end{aligned} \quad (34)$$

On the other hand, for the inverted hierarchy we find

$$P_{\omega,3}^0 = \int_0^{\omega_{\text{L}}^{\text{s}}} d\omega f(\omega) - \int_{\omega_{\text{L}}^{\text{s}}}^{\infty} d\omega f(\omega). \quad (35)$$

These relations allow us to calculate $\omega_{\text{H}}^{\text{s}}$ and $\omega_{\text{L}}^{\text{s}}$. Note that these results are exact only in the limit of an infinite mass-gap hierarchy, i.e., for $\alpha \rightarrow 0$, where the H and L splits perfectly factorize. Once the split frequencies have been found, the corresponding energies are $E_{\text{H}}^{\text{s}} = \Delta m_{\text{atm}}^2 / 2\omega_{\text{H}}^{\text{s}}$ and $E_{\text{L}}^{\text{s}} = \Delta m_{\odot}^2 / 2\omega_{\text{L}}^{\text{s}}$.

For our schematic SN model where the MSW level crossings and the spectral split region are widely separated, we find $E_{\text{H}}^{\text{s}} = 11.9$ MeV and $E_{\text{L}}^{\text{s}} = 16.9$ MeV in the normal hierarchy, and $E_{\text{L}}^{\text{s}} = 12.7$ MeV in the inverted hierarchy. We show the initial and final ν_e spectra for the Fermi-Dirac case in Fig. 10. Once more, we have coarse-grained over neighboring modes, representing the effect of kinematical decoherence.

VI. CONCLUSIONS

We have studied the three-flavor evolution of a ν_e burst that first undergoes two MSW level crossings driven by Δm_{atm}^2 and Δm_{\odot}^2 , respectively, and then undergoes spectral splits by the adiabatically decreasing strength of the neutrino-neutrino interaction. This case study of an MSW-prepared spectral split serves as a proxy for the

recent numerical study of the prompt ν_e burst in an O-Ne-Mg core collapse SN. Here, the matter density profile is so steep that the sequence between MSW crossings and collective neutrino oscillations is reversed from what would be expected in a traditional iron-core SN.

First we have analytically estimated the population of the propagation eigenstates after the MSW transformations. Due to the sharply falling matter density at the edge of the core of the star, the MSW transitions are not completely adiabatic, which helps in satisfying a precondition for the spectral splits to take place. We have used the well-known analytic double-exponential formula for calculating the jump probabilities.

We have studied numerically the subsequent spectral splits. We have analytically determined the split frequencies on the basis of two conserved flavor-lepton number combinations that supersede the single conservation law encountered in a two-flavor situation. The neutrino mass-gap hierarchy allows for a factorization of an H split and an L split, similar to the factorization of the MSW effect into an H and an L crossing. The dynamics of the split evolution is clearly seen to be a two-step process.

The dynamics of the two spectral splits can be understood in terms of the motion of the neutrino state in the \mathbf{e}_3 - \mathbf{e}_8 triangle diagram, which can explain many of the features of neutrino evolution qualitatively. The number of possible splits can be deduced by the location of the neutrino state inside the triangle. We have also shown how the positions of the splits can be calculated accurately given the initial neutrino spectra, and calculated the ν_e survival probability analytically, that matches the numerical computations.

Our analytic treatment accounts very nicely for the numerical findings of Duan et al. [34]. In their case the MSW conversion and the spectral splits are spatially very close so that it is not a priori obvious that our schematic model would be a good representation. In our treatment we have enforced a clear separation between the MSW region and the spectral-split region by assuming the limit of

large neutrino-neutrino interactions, a limit that also ensures that the MSW transition is perfectly synchronized and that the spectral split is perfectly adiabatic. A posteriori, however, our interpretation as a MSW prepared spectral split appears nicely justified and quantitatively appropriate. Our treatment is also a useful application of the three-flavor oscillation machinery developed by two of us recently [36].

It appears that the impact of collective neutrino oscillations on the propagation of the prompt ν_e burst is conceptually and quantitatively well under control. Characteristic signatures of these flavor transitions in large underground detectors have also been recently investigated [54]. What remains is to observe these features in the neutrino signal of the next galactic SN.

Note Added

After our manuscript was completed, a paper by Duan, Fuller and Qian appeared that treats three-flavor split phenomena [55]. The results partly overlap with our work.

Acknowledgments

In Munich, this work was partly supported by the Deutsche Forschungsgemeinschaft (grant TR-27 “Neutrinos and Beyond”), by the Cluster of Excellence “Origin and Structure of the Universe” and by the European Union (contract No. RII3-CT-2004-506222). In Mumbai, partial support by a Max Planck India Partnergroup grant is acknowledged. B.D. and A.D. also thank IMSc, Chennai, for their hospitality during WHEPP-X, when this work was completed. A.M. acknowledges support by the Alexander von Humboldt Foundation. A.M. acknowledges kind hospitality at the Tata Institute for Fundamental Research during the development of this work.

-
- [1] A. S. Dighe and A. Yu. Smirnov, “Identifying the neutrino mass spectrum from the neutrino burst from a supernova,” *Phys. Rev. D* **62**, 033007 (2000) [hep-ph/9907423].
 - [2] A. Dighe, “Neutrinos from a core collapse supernova,” [arXiv:0712.4386 [hep-ph]].
 - [3] R. C. Schirato and G. M. Fuller, “Connection between supernova shocks, flavor transformation, and the neutrino signal,” astro-ph/0205390 (unpublished).
 - [4] G. L. Fogli, E. Lisi, A. Mirizzi, and D. Montanino, “Analysis of energy- and time-dependence of supernova shock effects on neutrino crossing probabilities,” *Phys. Rev. D* **68**, 033005 (2003) [hep-ph/0304056].
 - [5] R. Tomàs, M. Kachelrieß, G. Raffelt, A. Dighe, H.-T. Janka and L. Scheck, “Neutrino signatures of supernova shock and reverse shock propagation,” *JCAP* **0409**, 015 (2004) [astro-ph/0407132].
 - [6] G. L. Fogli, E. Lisi, A. Mirizzi and D. Montanino, “Probing supernova shock waves and neutrino flavor transitions in next-generation water-Cherenkov detectors,” *JCAP* **0504**, 002 (2005) [hep-ph/0412046].
 - [7] B. Dasgupta and A. Dighe, “Phase effects in neutrino conversions during a supernova shock wave,” *Phys. Rev. D* **75**, 093002 (2007) [hep-ph/0510219].
 - [8] G. L. Fogli, E. Lisi, A. Mirizzi and D. Montanino, “Damping of supernova neutrino transitions in stochastic shock-wave density profiles,” *JCAP* **0606**, 012 (2006) [hep-ph/0603033].
 - [9] A. Friedland and A. Gruzinov, “Neutrino signatures of supernova turbulence,” astro-ph/0607244.
 - [10] D. Autiero *et al.*, “Large underground, liquid based detectors for astro-particle physics in Europe: scientific case and prospects,” *JCAP* **0711**, 011 (2007) [arXiv:0705.0116 (hep-ph)].

- [11] J. Pantaleone, “Neutrino oscillations at high densities,” *Phys. Lett. B* **287**, 128 (1992).
- [12] G. Sigl and G. Raffelt, “General kinetic description of relativistic mixed neutrinos,” *Nucl. Phys. B* **406**, 423 (1993).
- [13] S. Samuel, “Neutrino oscillations in dense neutrino gases,” *Phys. Rev. D* **48**, 1462 (1993).
- [14] V. A. Kostelecký and S. Samuel, “Neutrino oscillations in the early universe with an inverted neutrino mass hierarchy,” *Phys. Lett. B* **318**, 127 (1993).
- [15] V. A. Kostelecký and S. Samuel, “Self-maintained coherent oscillations in dense neutrino gases,” *Phys. Rev. D* **52**, 621 (1995) [hep-ph/9506262].
- [16] S. Samuel, “Bimodal coherence in dense selfinteracting neutrino gases,” *Phys. Rev. D* **53**, 5382 (1996) [hep-ph/9604341].
- [17] S. Pastor, G. G. Raffelt and D. V. Semikoz, “Physics of synchronized neutrino oscillations caused by self-interactions,” *Phys. Rev. D* **65**, 053011 (2002) [hep-ph/0109035].
- [18] Y. Y. Y. Wong, “Analytical treatment of neutrino asymmetry equilibration from flavour oscillations in the early universe,” *Phys. Rev. D* **66**, 025015 (2002) [hep-ph/0203180].
- [19] K. N. Abazajian, J. F. Beacom and N. F. Bell, “Stringent constraints on cosmological neutrino antineutrino asymmetries from synchronized flavor transformation,” *Phys. Rev. D* **66**, 013008 (2002) [arXiv:astro-ph/0203442].
- [20] S. Pastor and G. Raffelt, “Flavor oscillations in the supernova hot bubble region: Nonlinear effects of neutrino background,” *Phys. Rev. Lett.* **89**, 191101 (2002) [astro-ph/0207281].
- [21] R. F. Sawyer, “Classical instabilities and quantum speed-up in the evolution of neutrino clouds,” hep-ph/0408265.
- [22] R. F. Sawyer, “Speed-up of neutrino transformations in a supernova environment,” *Phys. Rev. D* **72**, 045003 (2005) [hep-ph/0503013].
- [23] H. Duan, G. M. Fuller and Y. Z. Qian, “Collective neutrino flavor transformation in supernovae,” *Phys. Rev. D* **74**, 123004 (2006) [astro-ph/0511275].
- [24] H. Duan, G.M. Fuller, J. Carlson and Y.Z. Qian, “Simulation of coherent non-linear neutrino flavor transformation in the supernova environment. I: Correlated neutrino trajectories,” *Phys. Rev. D* **74**, 105014 (2006) [astro-ph/0606616].
- [25] S. Hannestad, G.G. Raffelt, G. Sigl and Y.Y.Y. Wong, “Self-induced conversion in dense neutrino gases: Pendulum in flavor space,” *Phys. Rev. D* **74**, 105010 (2006) [astro-ph/0608695].
- [26] G.G. Raffelt and G. Sigl, “Self-induced decoherence in dense neutrino gases,” *Phys. Rev. D* **75**, 083002 (2007) [hep-ph/0701182].
- [27] H. Duan, G.M. Fuller, J. Carlson and Y.Z. Qian, “Analysis of collective neutrino flavor transformation in supernovae,” *Phys. Rev. D* **75**, 125005 (2007) [astro-ph/0703776].
- [28] G.G. Raffelt and A.Yu. Smirnov, “Self-induced spectral splits in supernova neutrino fluxes,” *Phys. Rev. D* **76**, 081301 (2007) [Erratum-ibid. *D* **77**, 029903 (2008)], [arXiv:0705.1830 (hep-ph)].
- [29] G.G. Raffelt and A.Yu. Smirnov, “Adiabaticity and spectral splits in collective neutrino transformations,” *Phys. Rev. D* **76**, 125008 (2007) [arXiv:0709.4641 (hep-ph)].
- [30] A. Esteban-Pretel, S. Pastor, R. Tomàs, G.G. Raffelt and G. Sigl, “Decoherence in supernova neutrino transformations suppressed by deleptonization,” *Phys. Rev. D* **76**, 125018 (2007) [arXiv:0706.2498 (astro-ph)].
- [31] H. Duan, G.M. Fuller and Y.Z. Qian, “A simple picture for neutrino flavor transformation in supernovae,” *Phys. Rev. D* **76**, 085013 (2007) [arXiv:0706.4293 (astro-ph)].
- [32] H. Duan, G.M. Fuller, J. Carlson and Y.Z. Qian, “Neutrino mass hierarchy and stepwise spectral swapping of supernova neutrino flavors,” *Phys. Rev. Lett.* **99**, 241802 (2007) [arXiv:0707.0290 (astro-ph)].
- [33] G.L. Fogli, E. Lisi, A. Marrone and A. Mirizzi, “Collective neutrino flavor transitions in supernovae and the role of trajectory averaging,” *JCAP* **0712**, 010 (2007) [arXiv:0707.1998 (hep-ph)].
- [34] H. Duan, G. M. Fuller, J. Carlson and Y. Z. Qian, “Flavor evolution of the neutronization neutrino burst from an O-Ne-Mg core-collapse supernova,” *Phys. Rev. Lett.* **100**, 021101 (2008) [arXiv:0710.1271 (astro-ph)].
- [35] A. Esteban-Pretel, S. Pastor, R. Tomàs, G. G. Raffelt and G. Sigl, “Mu-tau neutrino refraction and collective three-flavor transformations in supernovae,” *Phys. Rev. D* **77**, 065024 (2008) [arXiv:0712.1137 (astro-ph)].
- [36] B. Dasgupta and A. Dighe “Collective three-flavor oscillations of supernova neutrinos,” [arXiv:0712.3798 (hep-ph)].
- [37] S. Hannestad, H.-T. Janka, G. G. Raffelt and G. Sigl, “Electron-, mu-, and tau-number conservation in a supernova core,” *Phys. Rev. D* **62**, 093021 (2000) [astro-ph/9912242].
- [38] M. Kachelrieß, R. Tomàs, R. Buras, H.-T. Janka, A. Marek and M. Rampp, “Exploiting the neutronization burst of a galactic supernova,” *Phys. Rev. D* **71**, 063003 (2005) [astro-ph/0412082].
- [39] K. Nomoto, “Evolution of 8–10 M_{\odot} stars toward electron capture supernovae. I. Formation of electron-degenerate O + Ne + Mg cores,” *Astrophys. J.* **277**, 791 (1984).
- [40] K. Nomoto, “Evolution of 8–10 M_{\odot} stars toward electron capture supernovae. II. Collapse of an O + Ne + Mg core,” *Astrophys. J.* **322**, 206 (1987).
- [41] F.S. Kitaura, H.-T. Janka and W. Hillebrandt, “Explosions of O-Ne-Mg cores, the crab supernova, and subluminescent type II-P supernovae,” *Astron. Astrophys.* **450**, 345 (2006) [astro-ph/0512065].
- [42] H.-T. Janka, B. Müller, F. S. Kitaura and R. Buras, “Dynamics of shock propagation and nucleosynthesis conditions in O-Ne-Mg core supernovae,” [arXiv:0712.4237 (astro-ph)].
- [43] F. J. Botella, C. S. Lim and W. J. Marciano, “Radiative corrections to neutrino indices of refraction,” *Phys. Rev. D* **35**, 896 (1987).
- [44] C. Y. Cardall, “Liouville equations for neutrino distribution matrices,” arXiv:0712.1188 [astro-ph].
- [45] M.C. González-García and M. Maltoni, “Phenomenology with massive neutrinos,” [arXiv:0704.1800 (hep-ph)].
- [46] E. K. Akhmedov, C. Lunardini and A. Y. Smirnov, “Supernova neutrinos: Difference of ν_{μ} - ν_{τ} fluxes and conversion effects,” *Nucl. Phys. B* **643**, 339 (2002) [hep-ph/0204091].
- [47] A. B. Balantekin, J. Gava and C. Volpe, “Possible CP-violation effects in core-collapse supernovae,” [arXiv:0710.3112 (astro-ph)].
- [48] S. T. Petcov, “Exact analytic description of two neutrino oscillations in matter with exponentially varying density,” *Phys. Lett. B* **200**, 373 (1988).

- [49] P. I. Krastev and S. T. Petcov, “On the analytic description of two neutrino transitions of solar neutrinos in the sun,” *Phys. Lett. B* **207**, 64 (1988) [Erratum-ibid. *B* **214**, 661 (1988)].
- [50] G. L. Fogli, E. Lisi, D. Montanino and A. Palazzo, “Supernova neutrino oscillations: A simple analytical approach,” *Phys. Rev. D* **65**, 073008 (2002) [Erratum-ibid. *D* **66**, 039901 (2002)] [hep-ph/0111199].
- [51] A. Friedland, “On the evolution of the neutrino state inside the sun,” *Phys. Rev. D* **64**, 013008 (2001) [hep-ph/0010231].
- [52] E. Lisi, A. Marrone, D. Montanino, A. Palazzo and S. T. Petcov, “Analytical description of quasivacuum oscillations of solar neutrinos,” *Phys. Rev. D* **63**, 093002 (2001) [hep-ph/0011306].
- [53] M. Kachelrieß and R. Tomàs, “Non-adiabatic level crossing in (non-) resonant neutrino oscillations,” *Phys. Rev. D* **64**, 073002 (2001) [hep-ph/0104021].
- [54] C. Lunardini, B. Müller and H.-T. Janka, “Neutrino oscillation signatures of oxygen-neon-magnesium supernovae,” [arXiv:0712.3000 (astro-ph)].
- [55] H. Duan, G. M. Fuller and Y. Z. Qian, “Stepwise Spectral Swapping with Three Neutrino Flavors,” *Phys. Rev. D* **77**, 085016 (2008) [arXiv:0801.1363 [hep-ph]].